CATO-2 Deliverable WP3.4-D03

Development of chemical and mechanical experimental laboratory measurements

(Year 1 Progress Report)

Prepared by: Jon Samuelson
Bart Verberne
Colin Peach
Mariëlle Koenen
Xiaolong Zhang
Tjirk Benedictus
Jan ter Heege
Tim Tambach

Reviewed by: C.J. Spiers

Approved by: J.Brouwer
(CATO-2 Director)

1 Executive Summary (restricted)

One of the main concerns with geological storage of CO_2 is maintaining reservoir integrity in the face of leakage pathways due to wellbore perforations of the topseal or caprock. Previous experimental analyses vary widely in their predictions of the long term integrity of wellbore cement as a sealing agent for sequestration reservoirs. The focus of the experimental activities in WP3.4, is to advance the science of understanding the evolution of a wellbore seal of a CO_2 reservoir.

At Utrecht University (UU, HPT Laboratory), the focus of experimental activity lies on attempting to mimic key components of the entire wellbore system and measure changes in mineralogy and permeability of the wellbore system as a function of continued reaction and mechanical deformation in a CO_2 reservoir environment. In Year 1, UU has set up apparatus to conduct:

- Batch reaction experiments on powdered caprock mixed with powdered cement and ground casing steel to determine the long term, wellbore reaction products. These experiments will be conducted in a large volume autoclave over the course of up to 1 year under reservoir conditions.
- Permeability analyses on caprock cylinders to determine an initial state for the top seal of the P18 and other reservoirs. Experiments will predominantly be conducted using an Argon gas transient step technique at low confining pressures, with validation using an Argon flow through technique. Permeability will also be measured at in-situ confining pressure.
- Analyses on the evolution of the interfaces between caprock & cement and cement & casing steel. Experiments will be conducted on composite caprock-cement-steel samples. These will be subjected to CO_2 reservoir conditions for up to 1 year, and periodically analyzed for changes in bulk permeability, reaction progress and (interface) microstructure.
- Batch reaction experiments on varying mixtures of caprock, cement, and casing steel in a reaction vessel fitted inside of an Instron load frame under CO_2 reservoir conditions. This will be used to measure volume changes and swelling forces generated by reaction in the wellbore environment. Such effects may improve sealing but may also cause caprock fracture.

First results at UU using the Argon transient step method show that the permeability of the P18 caprock can vary from as high as 10^{-17} m^2 to far less than 10^{-19} m^2. There is currently no indication that permeability is strongly dependent on the formation of origin (Röt or Solling caprock) nor on orientation.

At the TNO-Rijswijk Prins Maurits Laboratory, the focus will be on investigating the long term effect of CO_2 reaction with cement and caprock, and clarifying the findings of previous studies. A new reaction vessel is being developed for this purpose that will very closely simulate the natural conditions of a CO_2 reservoir. The new experimental design is a great step forward in apparatus design for this type of experiment in that it provides a much more realistic reservoir environment by jacketing the reacted sample and subjecting it to static interaction with CO_2 and brine, rather than placing the sample in a brine bath and pressurizing the bath with CO_2.

At TNO Science and Industry (Den Helder), the contribution to WP3.4 is directed at corrosion studies. Supercritical CO_2 plus moisture or formation water in the CO_2 storage well environment forms carbonic acid that causes corrosion of tubes and casing steels, which combined with rock-cement interactions, may result in CO_2 leakage. Understanding steel corrosion under CO_2 storage conditions is critical to modelling well integrity. A preliminary desk study on the electrochemical measurements for tubing and casing steels in CO_2 environment has been done in the CATO-2 Year 1 program. In addition, the necessary experimental set-up for high pressure and high temperature (HPT) steel corrosion studies and the required electrochemical measurement protocol have been designed.

Distribution List

(this section shows the initial distribution list)

External	Copies	Internal	Copies

Document Change Record

(this section shows the historical versions, with a short description of the updates)

Version	Nr of pages	Short description of change	Pages

Table of Contents

2 Applicable/Reference documents and Abbreviations

2.1 Applicable Documents

(Applicable Documents, including their version, are documents that are the "legal" basis to the work performed)

	Title	Doc nr	Version date
AD-01	Beschikking (Subsidieverlening CATO-2 programma verplichtingnummer 1-6843	ET/ED/9078040	2009.07.09
AD-02	Consortium Agreement	CATO-2-CA	2009.09.07
AD-03	Program Plan	CATO2-WP0.A-D.03	2009.09.29

2.2 Reference Documents

(Reference Documents are referred to in the document)

	Title	Doc nr	Version/issue	Date

2.3 Abbreviations

(this refers to abbreviations used in this document)

3 General Text

3.1 INTRODUCTION

The basic concerns of the public regarding carbon capture and storage are "Will the CO_2 stay where it's put?" and "What risks are associated with putting it down there?" The laboratory work discussed here, falling under the auspices of CATO-2 Work Package 3.4: "Well integrity", focuses on the first of these concerns, specifically in regards to measuring what influence the caustic environment of a CCS reservoir has on wellbore integrity. We will analyze the mineralogical and structural changes that take place in the caprock, cement, and well casing, and also along the interfaces between these materials resulting from interaction with brine saturated CO_2.

Any depleted oil or gas reservoir used for the sequestration of CO_2 is likely to have been perforated many times by exploration and production wells. These wells are reinforced with a steel well casing held in place by an annular layer of cement between the caprock and the casing. Upon abandonment of the well after depletion of the hydrocarbons, or injection of CO_2, the wellbore is plugged with another volume of cement. Many experimental studies have been conducted analyzing the degradation of wellbore cement under CO_2 reservoir conditions [*Duguid et al.*, 2005; *Barlet-Gouedard et al.*, 2007; *Kutchko et al.*, 2007, 2008, 2009; *Strazisar et al.*, 2009], some suggesting that degradation of cement will be rapid while others suggest slower degradation. Examination of wellbore cements recovered from the SACROC Unit of West Texas, subjected to enhanced oil recovery practices for over 30 years, showed very low degradation rates [*Carey et al.*, 2007], implying that cement plugs may indeed be a sufficient barrier against the leakage of CO_2 from sequestration reservoirs.

The main concerns regarding CCS which will be addressed by our experimental analyses are as follows.

1) Many studies have been conducted that investigate the reaction of CO_2 with cement [see previous references], with caprock [*Rutqvist and Tsang*, 2002], and on well casing steel [*Wu et al.*, 2004; *Li et al.*, 2007]. To our knowledge however there have been no studies that examined the response of combined caprock, cement, and casing steel when subjected to CO_2 reservoir conditions. **What will be the products of reaction of a caprock, cement, steel system subjected to supercritical CO_2 and formation water? How fast will reactions proceed? What will be the relative roles of steel corrosion versus reactions between the various wellbore components?**

2) *Liteanu* [2009] showed that the permeability of cement decreases strongly with continued reaction with static CO_2 rich fluids, implying reduced porosity resulting from carbonation reactions in the cement inhibit internal fluid pathways. This would suggest that cement is an ideal material for plugging CO_2 reservoirs. Wellbores in actual reservoirs will not simply consist of cement, but a sandwich of cement, caprock, and casing steel, and the evolution of the interfaces between those materials will be of the utmost importance in maintaining the integrity of the reservoir. Recent work has shown that the interface between cement and a shale caprock is little affected by extended reaction with supercritical CO_2 [*Wigand et al.*, 2009], this would suggest that permeability of a combined caprock – cement system would decrease over time with the decreasing permeability of the cement. The influence of an evolving interfaces between the entire caprock, cement, and casing steel composite has yet to be investigated however. **What is the initial permeability of the caprock and the cement? How will the bulk permeability of a combined system of caprock – cement – casing steel evolve as a function of long term reaction with CO_2 and formation water? How will the interfaces between caprock & cement and cement & steel evolve over time in a CO_2 reservoir? What is the influence of mechanical deformation and stress changes?**

3) The products of the reaction of hydrated cement phases portlandite and calcium-silicate-hydrate with brine and supercritical CO_2 are calcite, aragonite, and vaterite all of which have larger molar volumes than portlandite, which results in a decrease in the porosity and permeability of the cement [*Wigand et al.*, 2009]. It is possible that the increase in volume of the cement will generate a force against the caprock and the steel well casing. By the same token it is possible that the reaction products of the entire caprock-cement-steel system could increase in overall volume, resulting in significant stresses in the wellbore that could ultimately fracture the caprock and result in loss of reservoir containment. **What volume change is associated with the reaction of caprock, cement, and casing steel with supercritical CO_2, what is the magnitude of the force developed as a result of this change in volume, and will reaction-swelling effects improve sealing capacity or cause caprock damage?**

Together, the HPT Lab at Utrecht University (UU), the Prins Maurits Laboratory of TNO in Rijswijk, and the TNO Science and Industry corrosion group in Den Helder, are in a unique position to be able to address all of these questions with in-house experimental equipment, and new, purpose-specific facilities under design, development and construction. We discuss below the contributions of these groups in Year 1 of CATO-2. This includes work on the caprock materials we have chosen to analyze, the formation fluid, and the experimental apparatuses to be used in elucidating the influence of supercritical CO_2 sequestration on all components of the caprock-cement-steel system.

3.2 UTRECHT UNIVERSITY WORK

SAMPLE MATERIALS AND PORE FLUID:

For our experimental work we intend to simulate chemically as well as structurally the injection point of a wellbore, the area of a potential CO_2 storage reservoir where wellbore integrity is most critical. The components that play a crucial role here are the impermeable

caprock roof of the reservoir, the steel casing that is used to support the well, the wellbore cement placed between the borehole and the casing, and finally the formation water pore fluid.

Caprock material:

Though the particular interest of this project is the potential effects of CO_2 sequestration on the P18 gas field [52°07'49"N 3°57'28"E], particularly wells P18-A-05 and P18-6A7, located approximately 18 km Northwest offshore Hoek van Holland, The Netherlands, we were unable to obtain caprock from those wells. As an analogue we have chosen material from the Röt and Solling claystones, the same geologic units as the suspected caprock in the P18 field, from the neighboring Q16 gas field, ~ 8 km offshore from Hoek van Holland [52°03'48"N 4°02'42"E]. We collected caprock samples from wells Q16-4 and Q16-FA-101-S1 from the TNO (Zeist) and NAM (Assen) core repositories respectively.

As shown in the drilling log lithostratigraphy available at the "NL Oil and Gas Portal" (http://www.nlog.nl/en/home/NLOGPortal.html) (Figure 1) the Röt and Solling formations provide the immediate cover to the Hardegsen, Detfurth, and Volpriehausen reservoir formations. In the P18 gas fields the Röt and Solling formations are located at approximately 4700 - 5100m depth, whereas in the Q16 field these same formations are found from approximately 3000 - 3500 m depth (Figure 1), perhaps due to faulting and partially to their closer proximity to the basin edge. Though located at very different depths it seems reasonable to conclude that the Röt and Solling formations in the P18 and Q16 well fields are mineralogically, structurally, and mechanically similar due to their close proximity to one another (~10 km apart).

We collected 14 samples from the Q16 gas field; 4 from well Q16-04 and 10 from well Q16-FA-101-S1 (Table 1; Figure 2). The depth range of the material from well Q16-04 is from ~ 3057 to 3067 m and in the Q16-FA-101-S1 well from ~ 3279 to 3292 m. Samples 8 – 15 have been prepared for permeability analysis, including cores drilled both perpendicular and parallel to the sedimentary layering. The samples were first cut and ground, yielding cylindrical 'plugs' of ~ 25 mm diameter, with sample lengths ranging from 10 to 20 mm.

Additionally we have begun conducting XRD analysis on samples 8 - 15, and will also attempt analysis on samples 53-60, should they be in an appropriate condition for study following their use in triaxial failure tests. The results of our ongoing analysis of the mineralogy of the caprock in the Q16 gas field show high phyllosillicate (muscovite) and carbonate (dolomite/ankerite) content (Table 2). It is interesting to note that samples 8 and 9, both from the Röt formation in well Q16-04 are very rich in muscovite (42-45%) with more modest amounts of ankerite (20-29%) whereas sample 13, extracted from the Q16-FA-101-S1 well, show the reverse, 52.5% ankerite and only 17.5% muscovite. Sample 12 is the only sample evaluated thus far that lies within the Solling formation, as defined by the lithostratigraphy (Figure 1), and it shows significantly different mineralogy from the Röt formation samples, dominated by dolomite (54%) and muscovite (39.7%), with very little quartz (3.3%) and ankerite (3%).

Steel casing:

The casing material used in the wells considered for CO_2 injection, i.e. wells P18-6A7 and P18-A-05, is API N80 grade steel. Through TNO Bouw & Ondergrond we obtained a weathered, tubular specimen of this material approximately 1.5 m long and 7.5 cm (3") in diameter. We cut off a short segments of the tube, approximately 5 cm long, from which we cut bars ~ 5 cm x 0.5 cm, and ground steel shavings (Figure 3A). The steel shavings were collected from freshly abraded steel and therefore do not contain corroded steel, whereas the rectangular bars were cut intentionally to have two corroded and two uncorroded sides. In this way the effect of CO_2 on corroded and uncorroded steel casing can be investigated and compared. The composition of uncorroded N80 grade steel is dominated by Fe (≥98%), with minor Mn (~1%), and trace amounts of C, Si, P, S, Mo, Cr, Ni, Nb, V, Ti and Cu [*Wu et al.*, 2004; *Li et al.*, 2009; *X. Zhang – TNO*, personal communication].

Wellbore cement:

The wellbore cement used in this study is API Class G Portland cement, which is widely used in oil and gas wells throughout the Netherlands. Presently we have cured and uncured type

G cement at our disposal, and both will be used in our experimental work. The cured cement is from an abandoned well of the RECOPOL ECBM field testing site in Southern Poland [*Van Bergen et al.*, 2006]. The uncured cement (Figure 3B) was obtained commercially, and will be mixed and cured following API Recommended Practice 10B in the near future.

Pore fluid:

The pore fluid brine used in this study is a solution of 2M NaCl + 0.2M $CaCl_2$ + 0.04M $MgCl_2$. This represents realistic reservoir brine, similar to that present in field P18 [*Bert de Wijn - Wintershall*, personal communication].

EXPERIMENTAL APPARATUS AND METHODS:

Composite caprock-cement-N80 steel cylinder:

In an effort to analyze the evolution of the entire wellbore system as it evolves in a supercritical CO_2 reservoir we will use a composite caprock-cement-steel cylinder to mimic the wellbore. The composite cylinder will consist of a hollow cylinder of caprock filled with Portland cement, with a bar of N80 steel standing vertically in the center (Figure 4). To simulate the conditions of a CO_2 reservoir the composite cylinder will be jacketed and placed in a high pressure and temperature hydrostatic reaction vessel (Figure 4). The jacketed sample will then be loaded hydrostatically and heated to reservoir conditions, saturated with formation water, and pressurized internally with supercritical CO_2. The cylinders will remain in the reaction chamber for up to 1 year, periodically being removed to measure the evolution of permeability of the simulated wellbore system as the cement, caprock, steel, and the interfaces between evolve in the reservoir environment. At the end of the experimental period the composite cylinders will be sliced in order to conduct microstructural analyses, focusing particularly on the evolution of the interfaces between caprock, cement, and steel.

Argon permeameter:

Knowing the permeability of the reservoir caprock and composite cylinder, and how it can change over the course of time when subjected to the corrosive conditions present in a CO_2 reservoir is one of the most fundamental questions regarding the CATO-2 project.

Using an argon gas permeameter (APE) (Figure 5) we have the ability to measure the permeability of cylindrical rock samples at low- and high-pressure conditions using two different methods. Using a small pressure vessel (labeled "LP" in Figure 5A) we can subject cylindrical samples to a confining pressure of up to 3.5 MPa at room temperature, and up to 100 MPa using a larger pressure vessel (labeled "HP" in Figure 5A), , both at room temperature. The LP-vessel is limited to samples 25 mm in diameter with length up to ~ 70 mm, and though the HP-vessel is currently set up for similarly sized samples, it could quickly be modified to accept much larger cores.

Using the APE we are able to conduct two very different types of permeability analysis, which allows us a simple method of validating any measurements that we make. The Argon-transient-step method (ATS) will be used most commonly in our analyses, and the values measured by ATS will be confirmed using the Argon-flow-through (AFT) method.

In both the ATS and AFT techniques the sample is placed between two end pieces (Figure 5B) which are grooved to ensure even distribution of the argon gas over the ends of the sample, and jacketed using a bicycle inner-tube (BIT) so that gas flows only along the axis of the cylindrical sample. The jacketed sample is then placed inside of the LP- or HP-vessel and a hydrostatic confining pressure is applied, sealing the edges of the sample ensuring that flow occurs only along the length of the core. Because the pressures that the samples are subjected to are hydrostatic the HP-vessel is capable of approximating in-situ stress conditions. The permeability of most samples will be measured in the LP-vessel using 2 MPa confining pressure, a few select samples will be run in the HP-vessel and if significant systematic variations in

permeability are detected as a function of confining pressure we will measure all samples in both the LP- and HP-vessels.

In the Argon-transient step method the sample is confined with 2 MPa confining pressure and then pressurized internally with ~ 1.6 MPa of Argon fluid pressure. Once the internal pore fluid pressure of the sample has equilibrated, a portion of the steel tubing of the APE is isolated from the sample, and reduced in pressure to ~ 1.4 MPa. The isolated low pressure portion of the APE tubing is then opened to the sample creating an instantaneous pressure transient across its length. By measuring the decay of the pressure imbalance between the upstream and downstream ends of the sample as they equilibrate towards a mean pressure of ~ 1.5 MPa, we are able to calculate the permeability (Figure 6). In order to correct for the Klinkenberg Effect we will also measure permeability at mean Argon pressures of 1.0 and 0.5 MPa (1.1 upstream/0.9 downstream & 0.6 upstream/0.4 downstream respectively) for very impermeable samples. Though current limitations in the ATS method prevent us from measuring permeability less than approximately 10^{-19} m^2, we hope to soon be able to measure permeability down to 10^{-21} m^2.

In addition to the ATS method we will use an Argon-flow-through (AFT) method of determining the permeability of our samples in order to validate the measurements made using the transient-step method. The AFT method is nominally a constant head permeability test, using Argon as the pore fluid. As with the ATS method the sample is loaded into either the LP- or HP-vessel and confining pressure is applied. The upstream side of the sample is attached to a large Argon gas reservoir, which is effectively infinite in volume compared to the pore volume of the sample. The downstream end of the sample is connected to a capillary tube at atmospheric pressure. When the upstream end is pressurized Argon gas will flow through the sample, and the volume of expelled gas is measured in the capillary tube. After a simple correction for the expansion of the Argon gas at atmospheric pressure the volume of expelled gas can be used in Darcy's Law to calculate the permeability of the sample and verify the findings of the more precise ATS method.

Autoclave and cold-seal batch reaction:

Using a 1-liter stainless steel autoclave fitted with an internal Teflon sleeve, we will react powdered volumes of samples 9 and 12-14, mixed with powdered Portland cement, and N80 steel shavings at near CO_2 reservoir conditions (30 MPa, ~100 °C) (Figure 7). Each mixture will be placed in one of four separate reservoirs in a Teflon reaction pot (Figure 7 – lower right). In order to mimic the natural conditions of the reservoir we will also include a small volume (~ 30 mL) of brine (2M NaCl, 0.2M $CaCl_2$, 0.04M $MgCl_2$) in the bottom of the autoclave well to simulate formation water. The autoclave will be opened every 4-6 weeks in order to harvest material from the other 4 Teflon pots (dedicated to WP3.3), at which time we will also gather small portions of the caprock-cement-steel mixtures in order to monitor the progress of the reactions over the course of 1 year.

A shortcoming of our autoclave technique for investigating the long term effect of CO_2 and brine on mixtures of caprock, cement, and casing steel is that there is no way to ensure that the reaction products of one of the sample pots will not influence the reactions in the other pots by way of dissolved transport through the wet supercritical CO_2. To investigate the reactivity of the caprock-cement-steel mixtures at CO_2 reservoir conditions in a more tightly controlled environment we will conduct batch reaction experiments on powdered caprock samples at in-situ pressure temperature conditions (115 °C, 35 MPa), similar to those conducted by *Hangx and Spiers* [2009] investigating the reaction of feldspar with CO_2. In this type of experiment a very small (~ 0.1 g) amount of the wellbore mixtures will be powdered and placed in a Teflon lined reaction vessel (Figure 8) along with a small volume of formation water. The reaction vessel is then fitted inside of a cold seal pressure vessel and attached to a pressurized source of CO_2 and brought to experimental pressure. A furnace is lowered over the pressure vessel and the sample is brought to experimental temperature. Though this type of experiment provides far better control on the reactive environment than the autoclave experiments it is more limited in its ability to provide a systematic analysis of the progression of reaction products for several different mixtures over very long time scales.

Instron – Force of crystallization:

To measure the possible force generated by changes in volume as the reactants in the caprock, cement, casing steel system react with one another in a reservoir environment we will conduct a series of force of crystallization (FOC) experiments in a reaction vessel fitted inside of an Instron load frame (Figure 9). A small amount of powdered sample (caprock, cement, N80 steel, and all combinations thereof) and formation water will be pressurized with supercritical CO_2 in the reaction vessel, and compressed vertically by a small constant load using the Instron load frame. As the sample volume changes the load frame will extend or retract as necessary to maintain the constant vertical load. By measuring the change in volume of the sample we can calculate the FOC for the combination of reactants in the chamber. The force generated by the reaction of the wellbore components could lead to reductions in permeability if the forces are modest and act as a self sealing mechanism for the wellbore, or if the forces are large they could result in fracturing of the caprock and loss of reservoir containment.

Triaxial testing machines:

To determine the effects of mechanical deformation and stress changes on cement samples, caprock samples and on the interfaces within composite samples of wellbore materials, exisiting triaxial testing facilities available at Utrecht will be used. These have been described in detail previously by *Liteanu* [2009] and are described in WP3.3-D08, so will not be addressed further here.

PRELIMINARY DATA AND NEXT STEPS:

Permeability data obtained so far show that the permeability of the caprocks ranges from roughly $1x10^{-17}$ m^2 to $5x10^{-19}$ m^2 (Table 2). Currently, more data is being collected, which will allow for a more thorough comparison, for example between the permeability measured on samples cored parallel and perpendicular to the sedimentary layering. Our next step in regards to

permeability measurement will be to complete the analysis across all samples and verify the measurements using the AFT method, and finally to measure a select group of samples at in-situ pressure conditions to determine if there is a large change in permeability based on confining pressure. Within a matter of weeks we anticipate having begun reaction experiments using the autoclave, cold seal, and Instron reaction vessels.

3.3 TNO-RIJSWIJK: STATIC REACTION EXPERIMENTS

This section describes the development of a laboratory facility at the Prins Maurits Laboratory of TNO in Rijswijk. The facility is developed to perform static reaction experiments between CO_2-rich brine and caprock as well as reservoir rock and wellbore cement at downhole/reservoir conditions. Development of the facility is therefore carried out within the framework of WP3.2 (Reservoir Behavior), WP3.3 (Caprock and Fault Integrity) and WP3.4 (Well Integrity).

An initial test facility was developed and used to carry out reaction experiments between CO_2-rich brine and wellbore cement (Figure 10). These experiments showed that some improvements to the setup were needed to reduce the brine to sample ratio and shield samples from the CO_2-rich brine acting as the pressure medium. Improvements to the setup and initial experiments on caprock samples are planned for year 2 of CATO-2.

An improved experimental setup is being developed which allows experiments with a more realistic brine to cement ratio (Figure 11). The main change to the initial setup is that an additional sample is placed between an upper and a lower stainless steel piston in an EPDM and FEP jacket and positioned next to a sample in the original sample configuration. Within the vessel a sample in the initial configuration can run simultaneous with a sample in the improved configuration in order to compare the two methods and to investigate the effect of the improved facility. A connection between the supercritical CO_2 in the open vessel and the jacketed sample is possible to allow equal CO_2 pressure and vaporized water content in both

experimental settings. The connection can also be closed in case a lower pressure is required in the jacketed sample to prevent leakage through the jacket. Experiments will have to show whether it is necessary to open the connection to prevent drying out of the jacketed sample and whether leakage in the jacketed sample will occur if the connection is opened. Brine samples can be taken during the experiment through the bleeding/sampling tap. The jacketed sample method is similar as used by *Liteanu* [2009] and therefore comparison of experimental results is allowed. The improved setup will shortly be used to perform experiments on representative samples of caprock and brine compositions (planned for year 2 of CATO-2).

3.4 TNO – DEN HELDER: CORROSION OF CASING STEEL IN CO_2 STORAGE ENVIRONMENTS

LITERATURE SURVEY

Literature related to the corrosion of steels in CO_2 transport and storage has been performed. Many factors affect the corrosion performance of the tubing and casing steels in CO_2. The composition and microstructure of materials, the application environment conditions, such as chemicals, pH, pressure, temperature, microorganism etc. have influence on the corrosion of the steels in the well.

Materials

The composition and microstructure of the materials have influence not only on the mechanical properties but also on the corrosion performance. Lopez et al. have reviewed the effect of microstructure and composition of carbon and low-alloyed steel on corrosion resistance in CO_2 environments (see Table 3) [1]. They found that even with apparently the same composition and microstructure, the performance of the carbon steels can vary greatly from the different suppliers.

Clover et al. studied the corrosion performance of various grades of carbon steels (ASTM A-106B, API 5L, L80, J55 etc.) in stirred (700 rpm) autoclaves using 1000 ml electrolyte with CO_2 at 50 °C for 2 weeks duration [2]. The carbon dioxide partial pressure is 3.4 bar, with the total pressure of 21 bar adjusted with methane. Corrosion and penetration rates were determined via mass loss and optical microscopy, respectively. The specimens were divided in 4 groups in different microstructures,
Group 1: banded ferrite/pearlite microstructure
Group 2: very fine predominantly ferrite microstructure

Group 3: ferrite/coarse and somewhat acicular pearlite/ pearlite microstructure
Group 4: tempered martensite microstructure

The localized and general corrosion rates vary slightly between different carbon steels (see Table 4).

Pfennig et al. have studied 42CrMo-4 and X46Cr13 in CO_2 saturated brine at 60 bar @60°C [3]. X46Cr13 shows a better corrosion resistance than 42CrMo-4, and their corrosion rate is different when exposed to the gas and to the liquid CO_2. However, pitting corrosion with pit depths about 1.4 mm after 2000 h were found on the X46Cr13 steel immersed in the liquid where the gas flow and pressure is low. CO_2 erosion-corrosion was found in the North Sea (Ekofisk) well No.2 oil well. The estimated average corrosion rate of the N-80 tubing is over 3 mm/y [4].

Effect of the pressure, temperature and pH

The pressure, temperature and pH value of the CO_2 in salt solution play critical roles in the corrosion of the materials. Seiersten and co-workers measured the corrosion rate for X65 low carbon steel in 10 g/l NaCl solution at 50°C as a function of CO2 pressure fugacity at semi-stagnant conditions with floating pH [5]. The corrosion rate increased with pressure and has a maximum of 6.9 mm/y at 40 bar, then decreased with pressure again. The corrosion rate increased with temperature and decreased with increasing pH.

Impurities in the CO_2

The presence of SO_x and NO_x in the CO_2 stream will significant increase the acidity of the aqueous phase. There is a need to understand the interaction of SO_x and NO_x with CO_2 under pressurized wet conditions, such as the effect of pH on the corrosion attack [6]. So far little experimental result concerning the impurity effect on the CO_2 corrosion under storage condition can be found in literature.

Microbiologically influenced corrosion (MIC)

Microbiologically influenced corrosion was not widely considered to be possible in downhole, though recognized in the pipeline industry for many years. Anaerobic sulfate reducing bacteria (SRB) and acid-producing bacteria (APB) can cause direct and indirect corrosion of the materials in down hole. Biological formations differ from rust in that they are shiny due to the formation of “biodome” [7]. The area under the biodome becomes anodic to the surface not covered by the biodome. Localized corrosion takes place under the biodome. The APB makes the local pH low and cause the local environment more corrosive. The SRB can reduce sulfate to sulfur which reacts with hydrogen to form hydrogen sulfide (H_2S). The H_2S can react with iron to produce iron sulfide, which can cause under-deposit corrosion. At the Ketzin storage project SRB bacteria have been found in the subsurface [8, 9].

Electrochemical measurements

Previous experimental data obtained in TNO show that the electrochemical impedance spectroscopy (EIS) and linear polarization resistance (LPR) measurements are useful to monitor the CO_2 corrosion, while the electrochemical noise measurements give large uncertainty [10]. From LPR we can estimate the corrosion rate of the materials in the specific environment. From EIS we obtain the corrosion resistance and the surface nature of the materials. The J55 steel (casing material) samples have been tested in 85 Bar @ 45°C in 102 g/L NaCl, 18g/L $CaCl_2$ and 9 g/L $MgCl_2$ solution. Strong variation in corrosion mechanism was observed after exposure the steel in the CO_2 solution. Some samples showed a passive surface (corrosion rate is low, ~ 0.6 mm/y) and some showed active surface (corrosion rate is high, ~ 8 mm/y).

In CO_2 storage well, localized corrosion is a more serious problem than uniform corrosion. The corrosion at the interface between casing steel and cement is also very dangerous to cause leak of CO_2 if corrosion of steel results in cracks. So, experimental investigation is deserved to understand the corrosion mechanism and to predict the service life of the casing or pipe materials.

EXPERIMENTAL SET-UP

The experimental set-up that works in high pressure (up to 300 bar) and high temperature (100°C) (HPT set-up) has been designed. Fig. 12 shows the HPT vessel and Fig. 13 shows the concept of the electrochemical cell. Electrochemical instruments, such as Ivium (conbined Potentiostat with Frequency Analyzer) can be used to monitor the electrochemical processes.

EXPERIMENTAL PLAN

Electrochemical measurements such as open circuit potential monitoring, potentiodynamic polarization (to study the Tafel slopes of the curves and the passivity of the materials), linear polarization measurements (to monitor the corrosion rate with time) and electrochemical impedance measurements will be carried out using the HPT set-up in different CO_2 environments. The objective of this study is to better understand the degradation mechanism of casing steel and tube materials in the CO_2 storage conditions.

Materials to be investigated: N80 steel, Cr13 steel
Electrolyte: 130 g/l NaCl, 22.2 g/l $CaCl_2$ and 4 g/l $MgCl_2$, representative to the well P18.
(1) Saturated with CO_2,
(2) CO_2 with impurities of SO_2 (0.05% by volume) and NO_2 (0.03% by volume)

Pressure: 60, 80, 100 bar
Temperature: 45, 60°C
pH: *in situ* control (pH sensor near the sample surface)

Electrochemical measurements:

OCP + LPR (±20 mV versus OCP)
OCP + EIS

Corrosion morphology analysis:
Topography (SEM)
Corrosion components on the surface (XRD)

Mass gain/loss measurements can be performed to calibrate the corrosion rate. Based on experimental results modeling of corrosion processes will be investigated.

ACKNOWLEDGEMENTS:

TNO Bouw & Ondergrond in Utrecht, the TNO core repository in Zeist and the NAM core repository in Assen are all kindly acknowledged for their help in retrieving the appropriate caprock samples. Further, the UU team would like to thank Peter van Krieken and Gert Kastelein for their assistance in designing and performing the lab experiments.

REFERENCES (SECTIONS 3.1 – 3.3):

Barlet-Gouedard, V., G. Rimmele, B. Goffe, and O. Porcherie (2007), Well Technologies for CO_2 Geological Storage: CO2-Resistant Cement, *Oil & Gas Science and Technology*, *62*, doi: 10.2516/ogst.2007027.

Carey, J. W., M. Wigand, S. J. Chipera, G. WoldeGabriel, R. Pawar, P. C. Lichtner, S. C. Wehner, M. A. Raines, and G. D. Guthrie Jr. (2007), Analysis and performance of oil well cement with 30 years of CO2 exposure from the SACROC Unit, West Texas, USA, *International Journal of Greenhouse Gas Control*, *1*, 75-85, doi: 10.1016/S1750-5836(06)0000-1.

Duguid, A., M. Radonjic, and G. Scherer (2005), Degradation of Well Cements Exposed to Carbonated Brine, *Conference Proceedings - Fourth Annual Conference on Carbon Capture and Sequestration DOE/NETL May 2-5, 2005*.

Hangx, S. J. T., C. J. Spiers, and C. J. Peach (2009), The mechanical behavior of anhydrite and the effect of CO_2 injection, *Energy Procedia*, *1*, 3485-3592.

Kutchko, B. G., B. R. Strazisar, D. A. Dzombak, G. V. Lowry, and N. Thaulow (2007), Degradation of Well Cement CO_2 under Geologic Sequestration Conditions, *Environmental Science & Technology*, *41*, 4787-4792.

Kutchko, B. G., B. R. Strazisar, G. V. Lowry, D. A. Dzombak, and N. Thaulow (2008), Rate of CO_2 Attack on Hydrated Class H Well Cement under Geologic Sequestration Conditions, *Environmental Science & Technology*, *42*, 6237-6242.

Kutchko, B. G., B. R. Strazisar, N. Huerta, G. V. Lowry, D. A. Dzombak, and N. Thaulow (2009), CO2 Reaction with Hydrated Class H Well Cement under Geologic Sequestration Conditions: Effects of Flyash Admixtures, *Environmental Science & Technology*, *42*, 3947-3952.

Li, D. G, Y. R. Feng, Z. Q. Bai, & M. S. Zheng, 2007, "Characteristics of CO2 corrosion scale formed on N80 steel in stratum water with saturated CO2" Applied Surface Science, 253, 8371-6

Liteanu, E. (2009), Subsurface Impact of CO2: Response of carbonate rocks and wellbore cement to supercritical CO2 injection and long-term storage, Utrecht University – Ph.D. Thesis, *Geologica Ultraiectina*, *310*, 184 pp.

Peach, C. J. (1991), Influence of deformation on the fluid transport of salt rocks, Utrecht University Ph.D. Thesis, *Geologica Ultraiectina*, *77*, 238 pp.

Rutqvist, J., and C. –F. Tsang (2002), A study of caprock hydromechanical changes associated with CO2-injection into a brine formation, *Environmental Geology*, *42*, 296-305.

Strazisar, B., B. Kutchko, and N. Huerta (2009), Chemical Reactions of Wellbore Cement Under CO2 Storage Conditions: Effects of Cement Additives, Energy Procedia, 1, 3603-3607, doi: 10.1016/j.egypro.2009.02.155.

Van Bergen, F., H. Pagnie & P. Krzystolik, 2006, "Field experiment of enhanced coalbed methane-CO2 in the upper Silesian basin of Poland.". Environm. Geosc., 13, 201-24

Wigand, M., J. P. Kaszuba, J. W. Carey, and W. K. Hollis (2009), Geochemical effects of CO2 sequestration on fractured wellbore cement at the cement/caprock interface, Chemical Geology, 265, 122-133, doi: 10.1016/j.chemgeo.2009.04.008.

Wu, S. L., Z. D. Cui, F. He, Z. Q. Bai, S. L. Zhu & X. J. Yang, 2004, "Characteristics of the surface film formed from carbon dioxid corrosion on N80 steel". Materials Letters, 58, 1076-81

REFERENCES (SECTION 3.4):

[1] D. A. López, T. Pérez and S. N. Simison, *Materials and Design*, 24, **2003**, 561.
[2] D. Clover, B. Kinsella, B. Pejcic, et al., *J. Appl. Electrochem.*, 35, **2005**, 139.
[3] A. Pfennig and R. Bäßler, *Corros. Sci.*, 51, **2009**, 931.
[4] C. J. Houghton and R. V. Westermark, *Materials perofrmance*, 22, **1983.**
[5] M. Seiersten and K. O. Kongshaug, in *Carbon Dioxide Capture for Storage in Deep Geologic Formations* D. C. Thomas and S. M. Benson Editors, Elsevier Ltd., **2005**, p. 937.
[6] B. Sass, B. Monzyk, S. Ricci, et al., in *Carbon Dioxide Capture for Storage in Deep Geologic Formations*, D. C. Thomas and S. M. Benson Editors, Elsevier Ltd., **2005**.
[7] C. L. Wheeler and D. L. Adams, Failure analysis of microbiologically influenced corrosion in middle eastern applications, in *Middle east artificial lift forum*, Muscat, Oman, **2002**, p. 24.
[8] D. Morozova, M. Wandrey, M. Alawi, et al., *Int. J. Greenhouse Gas Control*, **2010.**
[9] A. Myrttinen, V. Becker, R. van Geldern, et al., *Int. J. Greenhouse Gas Control*, **2010.**
[10] P. Bressers, R. Bisselink and J. Zevenbergen, Electrochemical monitoring steel corrosion during CO2 storage conditons, in, Eindhoven, **2008**.

P18-A-05

Kickoff Depth (m)	Bottom Hole Depth (m)	Stratigraphic Unit
0	974	North Sea Supergroup
974	2280	Ommelanden Formation
2280	2348	Texel Marlstone Member
2348	2440	Texel Greensand Member
2440	2726	Upper Holland Marl Member
2726	2812	Middle Holland Claystone Member
2812	2924	Holland Greensand Member
2924	3064	Lower Holland Marl Member
3064	3431	Vlieland Claystone Formation
3431	3462	Berkel Sandstone Member
3462	3549	Berkel Sand-Claystone Member
3549	3618	Rijswijk Member
3618	3717	Nieuwerkerk Formation
3717	4057	Lower Werkendam Member
4057	4487	Aalburg Formation
4487	4553	Sleen Formation
4553	4562	Upper Keuper Claystone Member
4562	4600	Dolomitic Keuper Member
4600	4610	Red Keuper Claystone Member
4610	4654	Upper Muschelkalk Member
4654	4667	Middle Muschelkalk Marl Member
4667	4681	Muschelkalk Evaporite Member
4681	4727	Lower Muschelkalk Member
4727	4775	Röt Claystone Member
4775	4787	Main Röt Evaporite Member
4787	4796	Solling Claystone Member
4796	4800	Basal Solling Sandstone Member
4800	4836	Hardegsen Formation
4836	4918	Upper Detfurth Sandstone Member
4918	4928	Lower Detfurth Sandstone Member
4928	5040	Upper Volpriehausen Sandstone Member
5040	5123	Lower Volpriehausen Sandstone Member
5123	5230	Rogenstein Member

P18-A-07-S1

Kickoff Depth (m)	Bottom Hole Depth (m)	Stratigraphic Unit
0	548	Upper North Sea Group
548	609	Vessem Member
609	862	Dongen Formation
862	1001	Landen Formation
1001	1883	Ommelanden Formation
Sidetrack		
1045	2140	Ommelanden Formation
2140	2203	Texel Marlstone Member
2203	2310	Texel Greensand Member
2310	2510	Upper Holland Marl Member
2510	2617	Middle Holland Claystone Member
2617	2740	Holland Greensand Member
2740	2887	Lower Holland Marl Member
2887	3266	Vlieland Claystone Formation
3266	3299	Berkel Sandstone Member
3299	3384	Berkel Sand-Claystone Member
3384	3478	Rijn Member
3478	3798	Alblasserdam Member
3798	4121	Werkendam Formation
4121	4199	Posidonia Shale Formation
4199	4730	Aalburg Formation
4730	4783	Sleen Formation
4783	4877	Keuper Formation
4877	4944	Muschelkalk Formation
4944	4954	Röt Formation
4954	4971	Solling Formation
4971	5002	Hardegsen Formation
5002	5052	Upper Detfurth Sandstone Member
5052	5066	Lower Detfurth Sandstone Member

Q16-04

Kickoff Depth (m)	Bottom Hole Depth (m)	Stratigraphic Unit
0	483	Upper North Sea Group
483	510	Middle North Sea Group
510	751	Lower North Sea Group
751	770	Ekofisk Formation
770	1407	Ommelanden Formation
1407	1459	Texel Formation
1459	1510	Texel Greensand Member
1510	1688	Upper Holland Marl Member
1688	1759	Middle Holland Claystone Member
1759	1797	Holland Greensand Member
1797	1865	Lower Holland Marl Member
1865	2106	Vlieland Claystone Formation
2106	2158	Berkel Sand-Claystone Member
2158	2169	Rijswijk Member
2169	2350	Werkendam Formation
2350	2385	Posidonia Shale Formation
2385	2850	Aalburg Formation
2850	2896	Sleen Formation
2896	2910	Upper Keuper Claystone Member
2910	2933	Dolomitic Keuper Member
2933	2943	Red Keuper Claystone Member
2943	2962	Upper Muschelkalk Member
2962	2981	Middle Muschelkalk Marl Member
2981	2987	Muschelkalk Evaporite Member
2987	3039	Lower Muschelkalk Member
3039	3064	Röt Claystone Member
3064	3071	Solling Claystone Member
3071	3076	Basal Solling Sandstone Member
3076	3136	Hardegsen Formation
3136	3162	Detfurth Claystone Member
3162	3167	Lower Detfurth Sandstone Member
3167	3216	Volpriehausen Clay-Siltstone Member
3216	3276	Lower Volpriehausen Sandstone Member
3276	3360	Rogenstein Member
3360	3462	Main Claystone Member
3462	3467	Zechstein Upper Claystone Formation
3467	3475	Z3 Fringe Sandstone Member
3475	3496	Z2 Fringe Sandstone Member
3496	3508	Z1 Fringe Sandstone Member
3508	3515	Z1 Lower Claystone Member
3515	3517	Fringe Coppershale Member
3517	3525	Slochteren Formation
3525	3714	Hellevoetsluis Formation
3714	3839	Maurits Formation

Q16-FA-101-S1

Kickoff Depth (m)	Bottom Hole Depth (m)	Stratigraphic Unit
0	476	Upper North Sea Group
476	516	Rupel Formation
516	822	Ieper Member
822	844	Basal Dongen Tuffite Member
844	897	Landen Clay Member
897	1657	Ommelanden Formation
1657	1702	Texel Marlstone Member
1702	1731	Texel Greensand Member
1731	1857	Upper Holland Marl Member
1857	1911	Middle Holland Claystone Member
1911	1967	Holland Greensand Member
1967	2098	Lower Holland Marl Member
2098	2216	De Lier Member
2216	2338	Eemhaven Member
2338	2367	IJsselmonde Sandstone Member
2367	2415	IJsselmonde Claystone Member
2415	2460	Berkel Sandstone Member
2460	2467	Berkel Sand-Claystone Member
2467	2520	Rijswijk Member
2520	2699	Nieuwerkerk Formation
2699	2716	Posidonia Shale Formation
2716	3117	Aalburg Formation
3117	3148	Sleen Formation
3148	3158	Upper Keuper Claystone Member
3158	3185	Dolomitic Keuper Member
3185	3192	Red Keuper Claystone Member
3192	3210	Upper Muschelkalk Member
3210	3221	Middle Muschelkalk Marl Member
3221	3226	Muschelkalk Evaporite Member
3226	3271	Lower Muschelkalk Member
3271	3292	Röt Claystone Member
3292	3302	Solling Claystone Member
3302	3304	Basal Solling Sandstone Member
3304	3374	Hardegsen Formation
3374	3399	Detfurth Claystone Member
3399	3405	Lower Detfurth Sandstone Member
3405	3451	Volpriehausen Clay-Siltstone Member
3451	3508	Lower Volpriehausen Sandstone Member
3508	3570	Rogenstein Member
3570	3636	Main Claystone Member
3636	3645	Zechstein Upper Claystone Formation
3645	3651	Z3 Fringe Sandstone Member
3651	3655	Grey Salt Clay Member
3655	3668	Z2 Fringe Sandstone Member
3668	3686	Z1 Fringe Sandstone Member
3686	3690	Z1 Fringe Carbonate Member
3690	3701	Coppershale Member
3701	3705	Slochteren Formation
3705	3970	Strijen Formation
3970	4023	Hellevoetsluis Formation
4023	4060	Maurits Formation

Figure 1 - Lithostratigraphy of wells P18-A-05 and P18-6A7 (considered for CO2 injection), and Q16-04 and Q16-FA-101-S1 (used for caprock sampling in this study). Note the different depth ranges of the reservoir (Volpriehausen, Detfurth, Hardegsen formations) and caprock (Solling and Röt formations) in the different wells.

UU Sample I.D.	Well I.D.	Depth (m)	Formation	XRD Results
8⊥ & 8//	Q16-04	3056.90 - 3056.97	Röt	45.1% - Muscovite - $KAl_2(AlSi_3O_{10})(OH)_2$ 28.6% - Ankerite - $Ca(Fe,Mg,Mn)(CO_3)_2$ 26.3% - Quartz - SiO_2
9⊥ & 9//	Q16-04	3060.78 - 3060.87	Röt	42.7% - Muscovite - $KAl_2(AlSi_3O_{10})(OH)_2$
				37.1% - Quartz - SiO_2
				20.3% - Ankerite - $Ca(Fe,Mg,Mn)(CO_3)_2$
10⊥ & 10//	Q16-04	3065.91 - 3065.97	Solling	Not yet evaluated
11⊥ & 11//	Q16-04	3066.53 - 3066.71	Solling	Not yet evaluated
12⊥ & 12//	Q16-FA-101-S1	3292,1	Röt/Solling	54.0% - Dolomite - $CaMg(CO_3)_2$ 39.7% - Muscovite - $KAl_2(AlSi_3O_{10})(OH)_2$ 3.3% - Quartz - SiO_2 3.0% - Ankerite - $Ca(Fe,Mg,Mn)(CO_3)_2$
13⊥ & 13//	Q16-FA-101-S1	3291,2	Röt	52.5% - Ankerite - $Ca(Fe,Mg,Mn)(CO_3)_2$ 30.4% - Quartz - SiO_2 17.1% - Muscovite - $KAl_2(AlSi_3O_{10})(OH)_2$
14⊥ & 14//	Q16-FA-101-S1	3290,05	Röt	Not yet evaluated
15//	Q16-FA-101-S1	3278,65	Röt	Not yet evaluated
53//	Q16-FA-101-S1	3289,75	Röt	Not yet evaluated
55//	Q16-FA-101-S1	3290,35	Röt	Not yet evaluated
56//	Q16-FA-101-S1	3290,6	Röt	Not yet evaluated
57//	Q16-FA-101-S1	3290,9	Röt	Not yet evaluated
59//	Q16-FA-101-S1	3291,5	Röt	Not yet evaluated
60//	Q16-FA-101-S1	3291,8	Röt/Solling	Not yet evaluated

Table 1 - Samples used in this study, including XRD data obtained thus far. ⊥ implies the sample is cored perpendicular to sedimentary layering. // implies the sample is cored parallel to the sedimentary layering.

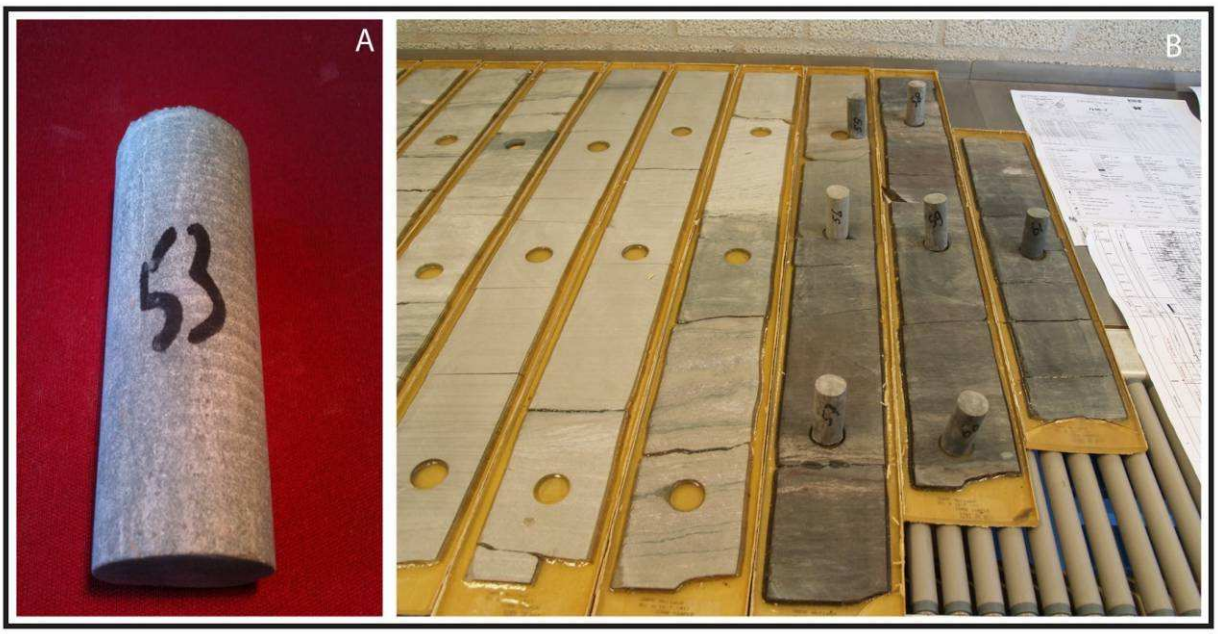

Figure 2 – A) Caprock sample 53 with a diameter of roughly 25 mm. B) Complete well core retrieved from well Q-16-FA-101-S1, displayed at the NAM core repository in Assen. The dark cores standing upright, originating from the Röt formation, were sampled as caprock material for this study.

UU Sample I.D.	*Permeability (m^2)*	
8⊥ & 8∥	⊥- n/a	∥- n/a
9⊥ & 9∥	⊥- $2.2x10^{-18}$	∥- n/a
10⊥ & 10∥	⊥- $0.41\text{-}5.5x10^{-18}$	∥- n/a
11⊥ & 11∥	⊥- n/a	∥- $0.17\text{-}2.7x10^{-17}$
12⊥ & 12∥	⊥- $0.50\text{-}4.2x10^{-18}$	∥- « 10^{-19}
13⊥ & 13∥	⊥- $1.0\text{-}7.4x10^{-18}$	∥- $4.9x10^{-18}$
14⊥ & 14∥	⊥- $0.47\text{-}1.3x10^{-17}$	∥- n/a
15∥	∥- n/a	
53∥	n/a	
55∥	n/a	
56∥	n/a	
57∥	n/a	
59∥	n/a	
60∥	n/a	

Table 2: Permeability data on the caprocks obtained thus far.

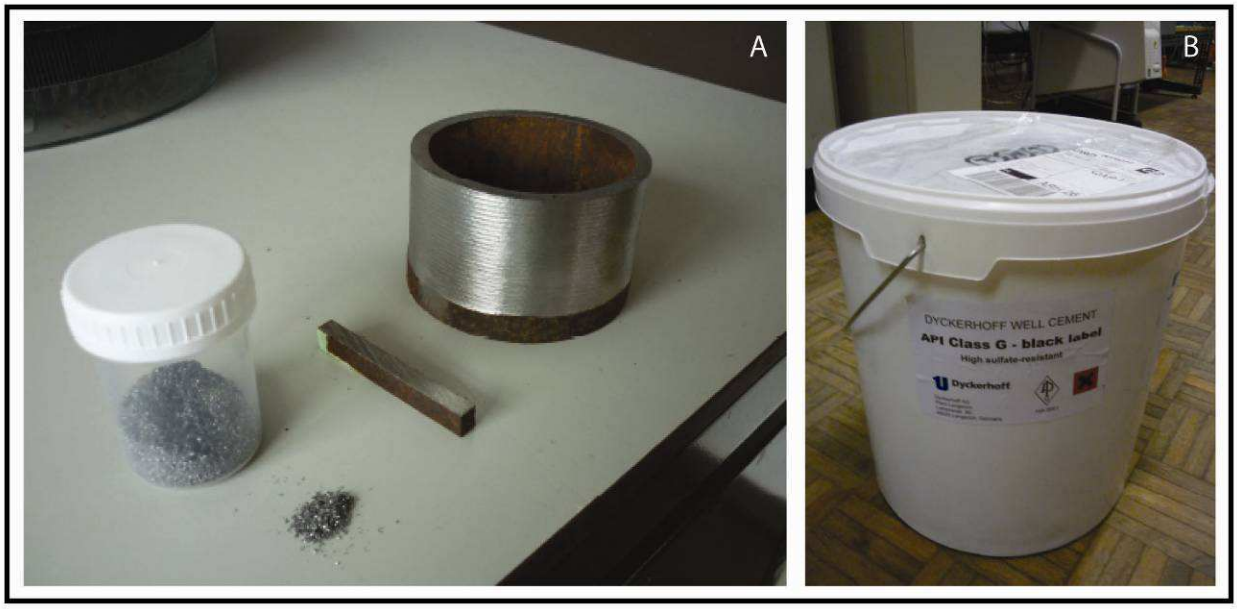

Figure 3 - A) N80 grade steel shavings (left), rectangular cut steel bars, and ground down steel tubing. B) Supply of uncured API class G wellbore cement.

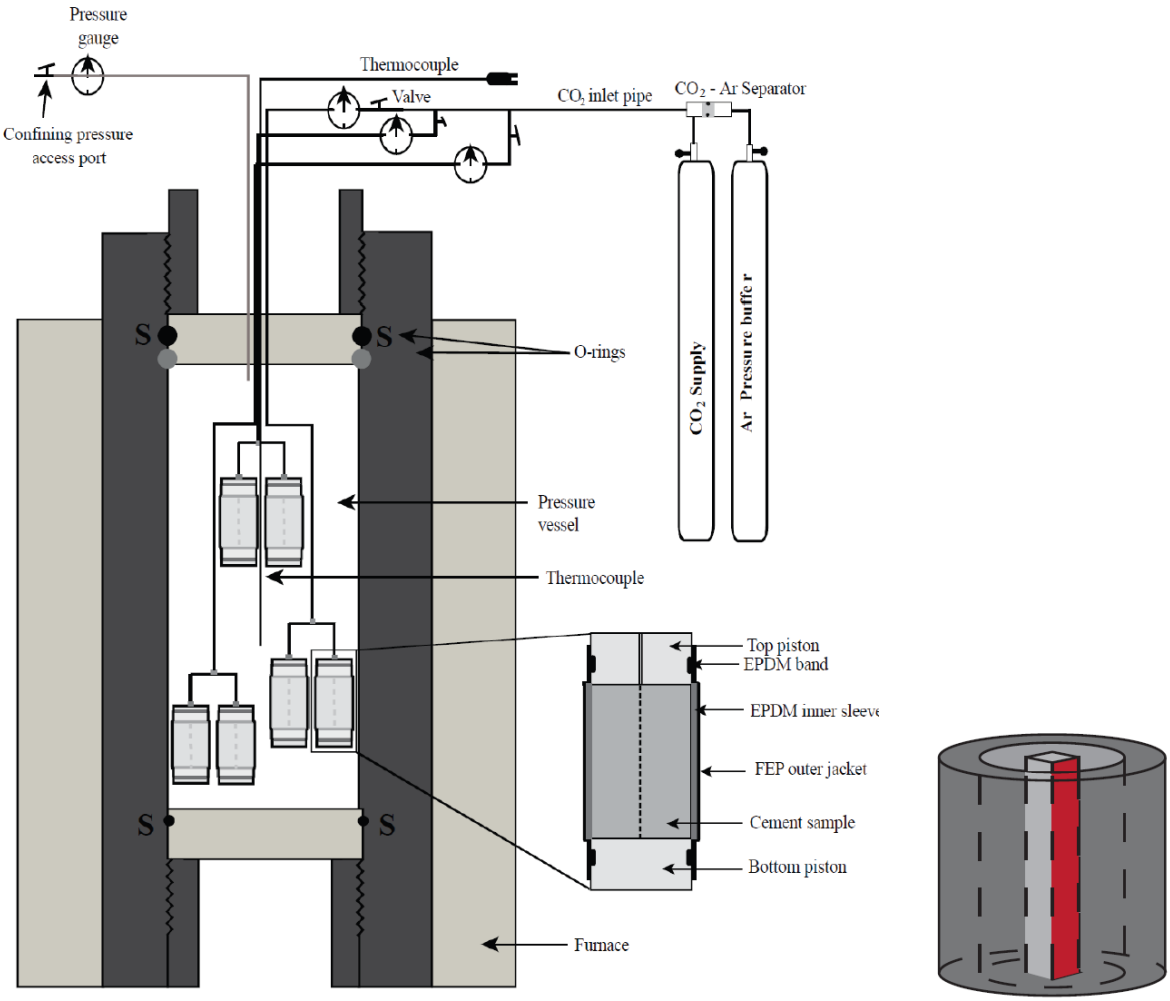

Figure 4 - We will use a high pressure and temperature hydrostatic reaction vessel to subject composite cylinders of caprock, cement, and casing steel to CO_2 reservoir conditions. The composite samples will consist of a hollow cylinder of caprock (dark grey in image above) filled with Portland cement (light grey), with a bar of N80 casing steel standing vertically in the center. The sample will be jacketed using a fluorinated ethylene propylene (FEP) shrink tube, and inserted into the reaction vessel. It will then be pressurized externally with a silicone base confining oil, saturated with formation water, and pressurzed internally with supercritical CO_2. Samples will be periodically removed from the vessel and measured for permeability changes using the Argon permeameter described later in this report. At the end of the experimental period the composite cylinders will be sliced in order to conduct a microstructural analysis on the interfaces between caprock & cement and cement & steel. [After *Liteanu*, 2009]

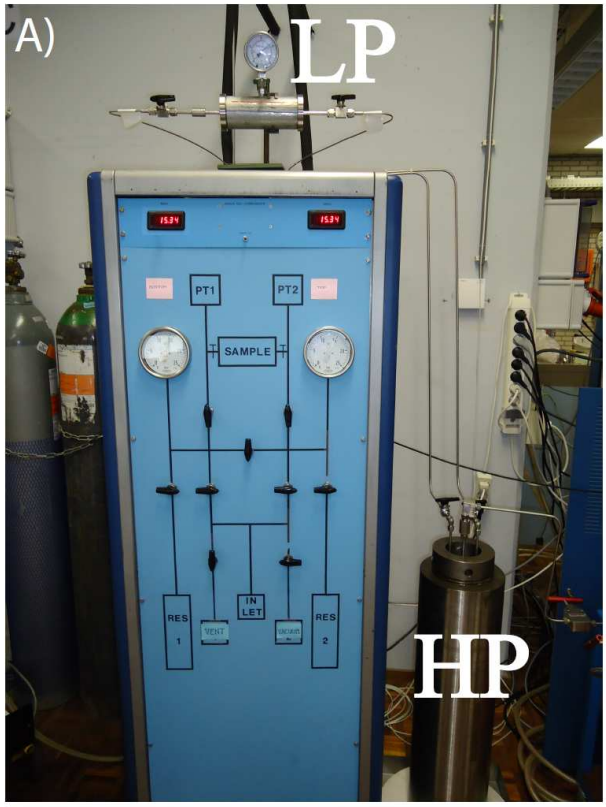

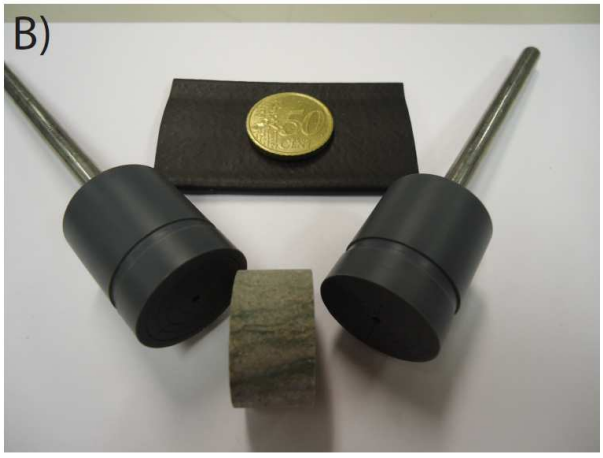

Figure 5 - A) Argon Permeameter (APE) used to make permeability measurements on all samples. Near the top of the APE is a low-pressure cell (labled "LP") used for confining 25 mm diameter cylindrical samples up to ~70 mm in length, at up to 3.5 MPa. On the right hand side of the APE is a recently developed high-pressure cell (labeled "HP") which can be pressurized up to 100 MPa and used to measure the permeability of cap rock and reservoir samples at in-situ pressure conditions. Current procedures limit our ability to measure samples with permeability much lower than ~10^{-19} m^2, but these limitations should be overcome in the near future. B) Sample holders are grooved to allow even distribution of argon gas over the surface of the ends of the sample. Bicyle inner-tube (beneath coin) is used as a jacketing membrane to isolate the sample from the confining pressure, ensuring flow of Argon gas occurs only along the axis of the sample. Sample 14 is shown here also.

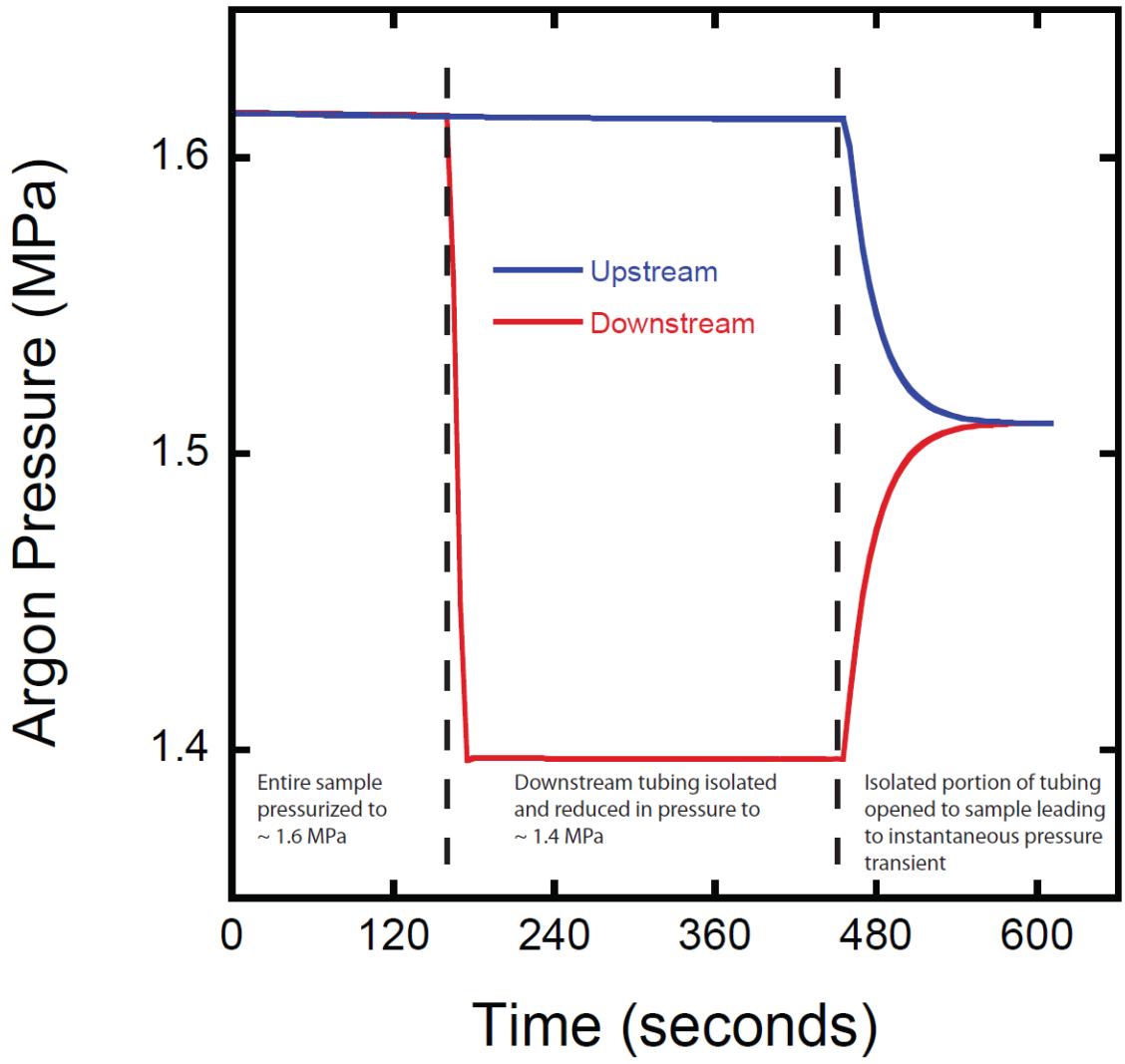

Figure 6 - Results of an Argon-transient-step permeability test in APE LP-vessel. The sample is initially pressurized with approximately 1.6 MPa of Argon fluid pressure. Once the fluid pressure in the sample has equilibrated the downstream side of the APE tubing is isolated from the sample and reduced in pressure to approximately 1.4 MPa. The isolated low-pressure tubing is then opened to the sample, resulting in an instantaneous pressure transient across the sample which decays over time. By measuring the decay of the pressure imbalance across the sample we are able to calculate the permeability.

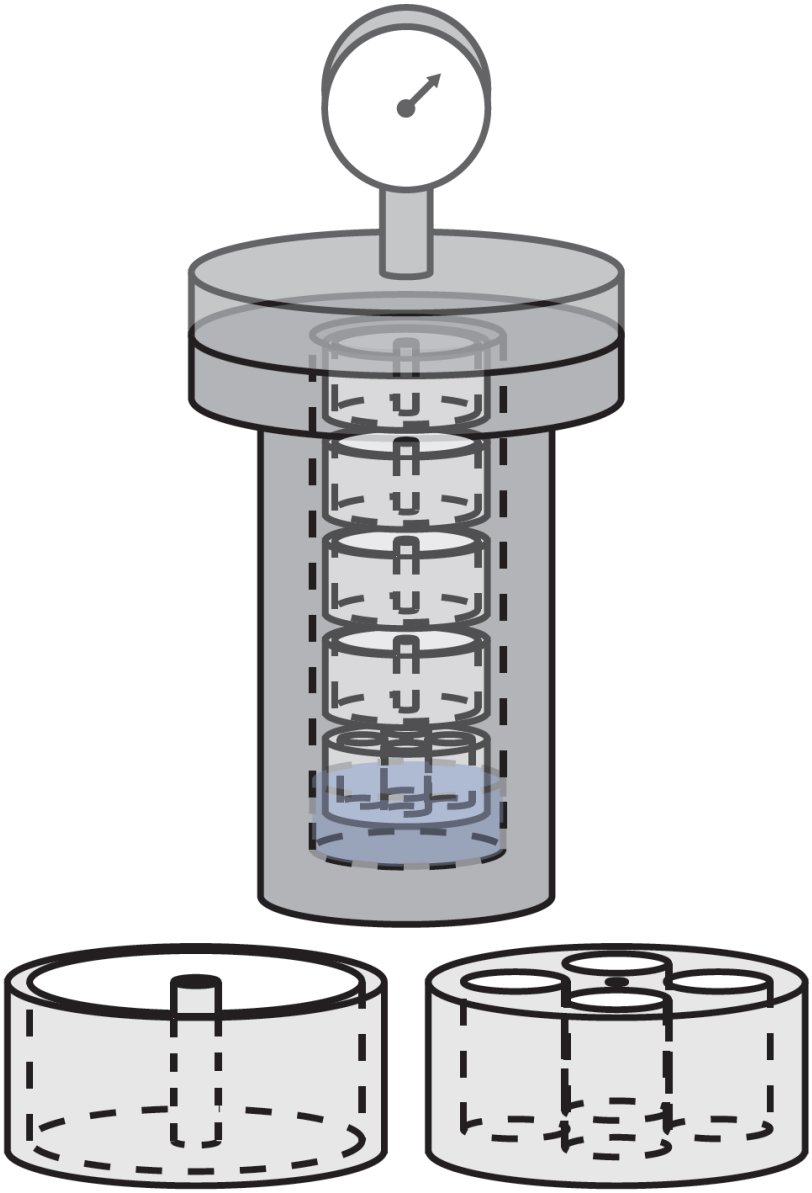

Figure 7- Schematic diagram of batch autoclave reaction experiments. Caprock samples 9 and 12-14 have been powdered and will be mixed with powdered Portland cement and shavings of N80 casing steel. These mixed samples will then be placed one of four seperate reservoirs in a Teflon pot (lower right), and placed inside of a 1-liter autoclave reaction vessel along with ~ 30 mL of formation water (2M NaCl, 0.2M $CaCl_2$, 0.04M $MgCl_2$). The autoclave will then be pressurized with 30 MPa CO_2 pressure and heated to ~ 100 ^{o}C. The autoclave will be opened every 4-6 weeks to harvest material from the remaining for Teflon pots which are used in WP3.3, at which time we will also harvest material from the caprock-cement-steel mixtures in order to monitor the progress of the reaction over the course of up to 1 year.

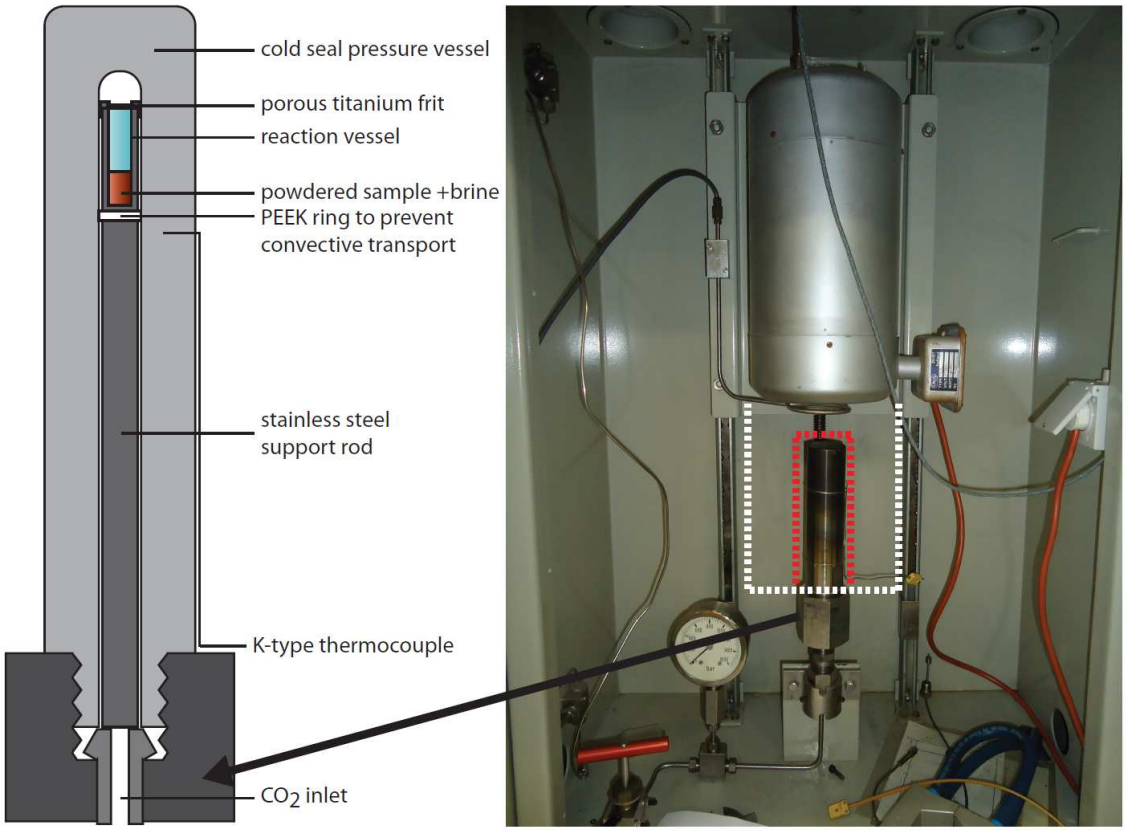

Figure 8 - Cold-seal pressure vessel used for reaction of caprock/cement/steel mixtures. Samples of ~ 0.1 g are heated and pressurized with CO_2 to in-situ conditions (35 MPa, 115 °C). The duration of experiments can be systematically controlled in order to determine at what point during CO_2 sequestration mineral assemblages may form. The photograph shows the cold seal pressure vessel in place (outlined in red) before the furnace has been lowered into place over the pressure vessel (outlined in white).

Figure 9 - Force of crystalization experiments are conducted in a reaction vessel fitted into an Instron load frame. A small sample of a combination of powdered caprock, cement, and ground N80 steel is pressurized with supercritical CO_2 and allowed to react under a small constant vertical load. As the sample swells due to reaction with CO_2 over the course of the experiment, the load frame will retract in order to maintain the set vertical load. By measuring the change in volume of the sample we are able to calculate a so-called force of crystallization, which may be of significant importance in potentially fracturing the caprock, leading to loss of containment of the CO_2 reservoir.

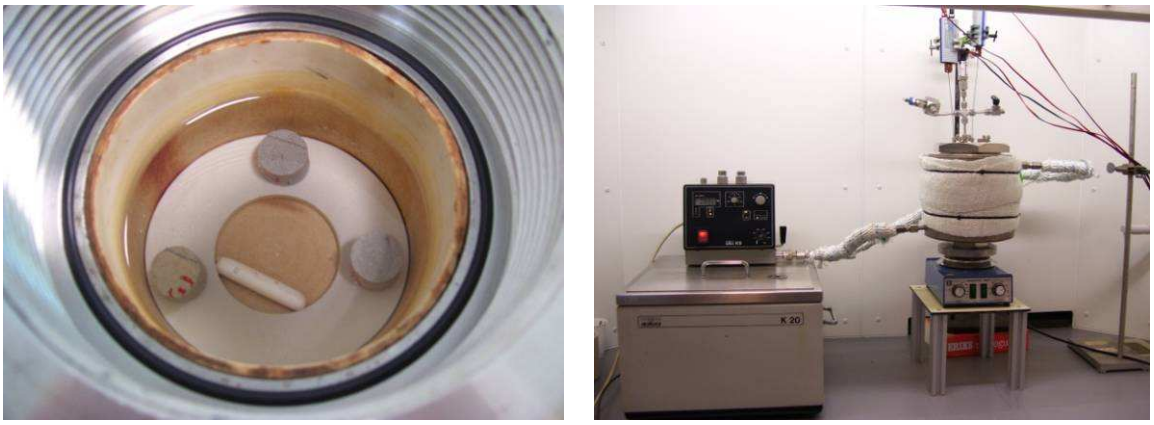

Figure 10 - Left: Pressure vessel and Teflon reservoir containing 3 small cement samples, brine and a stirring device. Right: Experimental setup with the heat bath on the left and the vessel on the right, isolated by glass wool. Thermocouples and pressure measurement devices are placed on the cover of the pressure vessel and attached to a computer to monitor pressure and temperature of the brine and the supercritical CO_2 during the experiments.

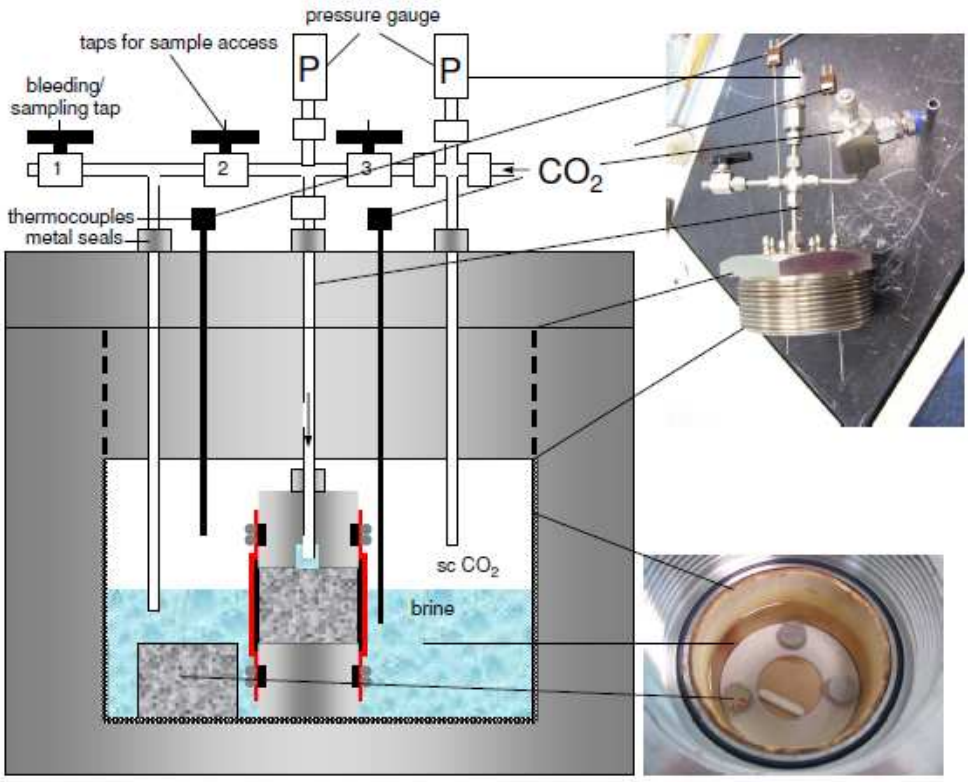

Figure 11 – Sketch of improved TNO – Rijswijk autoclave apparatus

Table 3 Chemical composition in wt% and microstructure of steel [1].

Chemical composition (wt.%) and microstructures of the steels employed in the cited papers

Reference	Material	C	Mn	Si	S	P	Cr	Ni	Cu	Mo	Al	Ti	Nb	Microstructure
Nesic et al. [11]	St52	0.065	1.54	0.25	0.001	0.013	0.05	0.04	0.04	0.0007	0.041	–	–	–
	X65	0.13	1.25	0.35	0.004	0.022	0.12	0.08	0.31	0.02	0.035	–	–	–
Palacios and Shadley [45]	API N80	0.29	1.48	0.34	0.0014	0.012	0.24	0.08	<0.01	0.09	0.04	<0.01	–	M
	API N80	0.33	1.59	0.41	0.017	0.016	0.58	0.09	<0.01	0.24	0.04	<0.01		F/P
	UNS G10180	0.15–0.20	0.60–0.90	–	0.05	0.04	–	–	–	–	–	–	–	F/P
M. Ueda and H. Takabe [6]	J55	0.52	0.96	0.33	<0.011	<0.01	0.17	0.04	0.09	0.02	–	–	–	F/P
	N80	0.23	1.38	0.21	0.013	0.023	0.05	–	–	–	–	–	–	M
López et al. [39,40]	J55	0.38	0.99	0.33	<0.01	<0.01	0.17	0.04	0.09	0.02	---	–	–	F/P and M
Al Hassan et al. [47]	API X52	0.14	1.26	0.22	0.002	0.018	–	–	–	–	–	–	0.022	F/P, M and TM
	UNS J22090	0.08	0.83	0.52	0.006	0.022	2.3	–	–	1.37	–	–	–	F/P, TB, BF and B
	UNS G10800	0.78	1.26	0.22	0.02	0.03	–	–	–	–	–	–	–	P and M
Dugstad et al. [19]	St52	0.15	1.57	0.18	0.011	0.014	0.03	0.04	0.015	–	–	–	–	F/P, S, M and TM
	Cr0.87	0.18	1.08	0.31	0.029	0.01	0.87	0.09	0.12	–	–	–	–	F/P, M and TM
	Cr0.53	0.06	1.12	0.24	0.003	0.008	0.53	0.02	<0.01	–	–	–	–	F/P and B
Mora-Mendoza et al. [41]	–	0.148	0.799	0.175	0.032	0.010	0.069	0.065	–	0.014	–	–	–	F/P
E. Gulbrandsen et al. [21]	X65	0.064	1.55	0.26	0.001	0.012	0.05	0.04	0.04	0.01	0.041	–	0.041	F/P
	St52	0.13	1.29	0.38	0.008	0.015	0.07	0.09	0.34	0.01	0.05	–	–	F/P
	Cr0.5	0.072	0.89	0.17	0.002	0.014	0.6	0.02	0.01	0.01	0.038	–	–	FW
Kapusta and Canter [60]	N80	0.22	0.90	–	–	–	0.6	–	–	0.15	–	–	–	TM
	J55	0.45	1.00	–	–	–	–	–	–	–	–	–	–	F/P
Gulbrandsen et al. [49]	16 steels (named A to P)	0.035–0.15	0.6–1.54	0.07–0.43	0.001–0.022	0.007–0.021	0.01–0.16	0.03–0.26	0.02–0.34	0.01–0.15	0.01–0.05	–	0–0.043	F/P and TM

F: ferrite, P: pearlite, M: martensite, T: tempered, B: bainite, S: spheroidite, W: wiedmanstatten.

Table 4 Corrosion resistances of steel specimens grouped according to microstructure [2].

Microstructural group [2] (No. of samples in group)	Mean penetration rate (Range) mm/y	Mean average corrosion rate (Range) mm/y
Group 1 (4)	6.0 (5.7–6.4)	1.7 (1.0–2.2)
Group 2 (7)	4.5 (3.9–5.2)	1.5 (1.0–3.2)
Group 3 (5)	4.7 (3.3–6.0)	1.2 (0.8–1.6)
Group 4 (2)	4.5 (4.4–4.6)	2.1 (2.0–2.2)

Fig. 12: The HPT vessel used for the corrosion experiments.

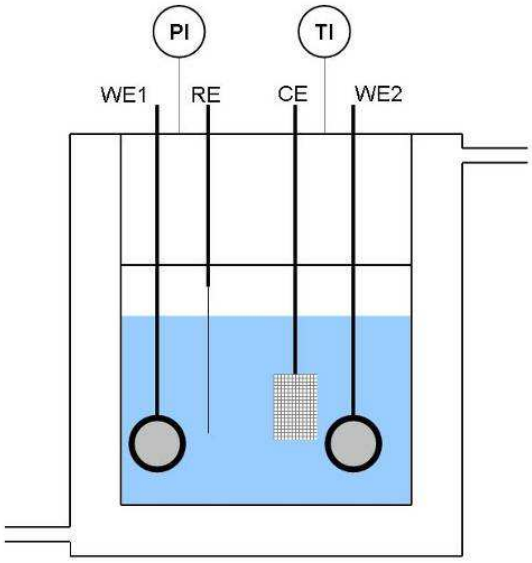

Fig. 13: Schematic illustration of the electrode configuration inside the HPT set-up. WE1 and WE2 are both working electrodes made from materials to be studied. The second working electrode is needed for duplicate measurements or for possible electrochemical noise measurements. The counter electrode (CE) is made from a Pt wire gauze. The reference electrode (RE) is Ag/AgCl saturated with KCl solution.